J. Fluid Mech. (2007), *vol.* 585, *pp.* 487–497.
doi:10.1017/S0022112007007033 Printed in the United Kingdom

Polymer mixing in shear-driven turbulence

T. VAITHIANATHAN[1]†, ASHISH ROBERT[2], JAMES G. BRASSEUR[2] AND LANCE R. COLLINS[1]‡

[1]Sibley School of Mechanical & Aerospace Engineering, Cornell University, Ithaca, NY 14853–7501, USA

[2]Department of Mechanical & Nuclear Engineering, The Pennsylvania State University, University Park, PA 16802, USA

(Received 21 January 2007 and in revised form 21 May 2007)

We investigate numerically the influence of polymer mixing on shear-driven turbulence. Of particular interest is the suppression of mixing that accompanies drag reduction with dilute polymer solutions. The simulations use the finite extensible nonlinear elastic model with the Peterlin closure (FENE-P) to describe the polymer stresses in the momentum equation, with polymer concentration allowed to vary in space and time. A thin slab of concentrated polymer was placed in an initially Newtonian homogeneous turbulent shear flow on a plane perpendicular to the mean velocity gradient, and allowed to mix in the gradient direction while actively altering the turbulence. The initially higher concentration of polymer near the centreplane suppressed production of turbulent kinetic energy and Reynolds stress in that region, while turbulence outside the polymer-rich region remained shear-dominated Newtonian turbulence. The rate of mixing in the shear direction was severely damped by the action of the polymer compared to a passive scalar in the corresponding Newtonian turbulent shear flow. This, in part, was a result of the same damping of vertical velocity fluctuations by the polymer that leads to the suppression of momentum flux. However, the cross-correlation between the polymer concentration and vertical velocity fluctuations was also suppressed, indicating that the explanation for the reduction in polymer mixing involves both the suppression of vertical velocity fluctuations and an alteration of turbulence structure by the polymer–turbulence interactions.

1. Introduction

Direct numerical simulations (DNS) of polymer–turbulence interactions have been performed in isotropic turbulence (De Angelis *et al.* 2005), homogeneous shear flow (Robert *et al.* 2007), turbulent channel flow (Sureshkumar, Beris & Handler 1997; Min *et al.* 2003; Ptasinski *et al.* 2003; Dubief *et al.* 2004), and boundary layers (Dimitropoulos *et al.* 2005). These studies modelled the polymer stress with the closed finite extensible nonlinear elastic equation (FENE-P) derived by Peterlin (1961), and assumed a uniform polymer concentration throughout the domain. However, the application of polymer drag-reduction technology to the boundary layer of ships and submarines, for example, includes mixing of the injected polymer normal to the surface. This aspect of the problem was recently investigated numerically by Dimitropoulos *et al.* (2006), who observed a decrease in the percent drag reduction

† Present address: Clear Science Corp., 663 Owego Hill Rd., Harford, NY 13784-0233, USA
‡ Author to whom correspondence should be addressed. LC246@cornell.edu

in the inhomogeneous polymer case compared to uniform polymer concentration at the wall value.

Experimental investigations of polymer drag reduction have also, largely focused on uniform polymer concentration (Virk 1975). Experiments with polymer injection have been directed towards polymer mixing and the persistence length of drag reduction (Petrie & Fontaine 1996; Somandepalli 2006). More fundamental studies aimed at isolating the effect of the polymer on the bulk turbulence from the near-wall surface layer also have been undertaken (McComb & Rabie 1982; Bewersdorff *et al.* 1993; Cadot, Bonn & Douday 1998). The issue is complicated by the fact that polymers, injected at relatively high concentrations, can aggregate into filaments that are remarkably effective drag-reducing agents both in the bulk flow and near the wall (Bewersdorff *et al.* 1993). McComb & Rabie (1982) and recent experiments by Bonn *et al.* (2005) identify the surface layer as the primary source of polymer drag reduction, although the effect can reach the centre of the channel, depending on the choice of parameters (L'vov *et al.* 2004).

A related problem of some practical significance is the transport of a passive scalar such as temperature in heating/cooling systems that use drag-reducing agents to reduce pumping costs. Studies have shown that a reduction in the heat transfer coefficient accompanies drag reduction (Cho & Hartnett 1982; Yoon & Ghajar 1987). Gupta, Sureshkumar & Khomami (2005) used DNS to show that the reduction is correlated with the attenuation of the wall-normal velocity fluctuations by the polymer.

Recently, our group has developed a direct numerical simulation of homogeneous turbulent shear flow with polymers modelled by the FENE-P equation (Vaithianathan *et al.* 2006). Homogeneous shear flow is perhaps the most fundamental flow that includes the essential physics underlying polymer-induced reductions in Reynolds stress relative to Newtonian turbulence. We seek a fundamental understanding of the mechanism of drag reduction, and we argue that this flow provides a description of the most basic physics that underlies the suppression of the turbulent momentum flux that leads to drag reduction in wall-bounded flows. For the homogeneous polymer concentration case (Robert *et al.* 2007), the transport terms are eliminated, revealing directly the actions of the polymer on shear-dominated turbulence without the complicating factors such as blockage and viscous-dominated wall layers at boundaries. With appropriately chosen shear rates, homogeneous shear flow is a good model of the inertial sublayer of a turbulent boundary layer (Lee, Kim & Moin 1990). Hence it is an important 'building block' flow for fundamental analysis and modelling of drag reduction. For example, Robert *et al.* (2007) showed how polymer–turbulence interactions with shear produce a realignment of component turbulent kinetic energy that weakens Reynolds stress production.

In this study, we modify the earlier simulations to investigate the mixing of active polymer by turbulence using the same shear flow simulation tool as Vaithianathan *et al.* (2006). We apply the FENE-P model for the polymer stress in a form that allows the polymer concentration to vary in space and time. A polymer layer is initially concentrated in a thin slab perpendicular to the direction of the mean velocity gradient. We are interested in the transport of polymer in the mean gradient direction, similar to polymer that has been injected into a boundary layer through a slot in the wall (Petrie & Fontaine 1996; Somandepalli 2006; Dimitropoulos *et al.* 2006). We investigate the rate of mixing of the polymer slab and compare it to the equivalent mixing of a passive scalar in Newtonian shear flow. We also explore the dependence of the mixing process on the polymer relaxation time (Weissenberg number) and maximum extensibility parameter. The results provide a quantitative measure of

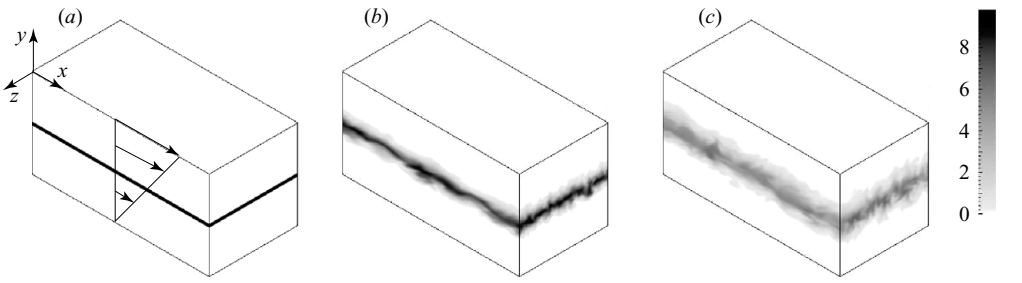

FIGURE 1. Isocontours of polymer concentration on the outer surface of the computational domain for case A at (*a*) $\mathscr{S}t=0$; (*b*) $\mathscr{S}t=6$; and (*c*) $\mathscr{S}t=12$. Profiles across the mixing layer are obtained by averaging over x–z planes (i.e. homogeneous directions).

the effect of the polymers on mixing in a simple (statistically one-dimensional) geometry, and hence are complementary to the more complex (two-dimensional) mixing scenarios found in channel flows (Gupta *et al.* 2005) and boundary layers (Dimitropoulos *et al.* 2006).

2. Governing equations and problem specification

The momentum equation for a dilute polymer solution is

$$\frac{\mathrm{D}\boldsymbol{u}}{\mathrm{D}t} \equiv \frac{\partial \boldsymbol{u}}{\partial t} + \boldsymbol{u}\cdot\nabla\boldsymbol{u} = -\frac{1}{\rho}\nabla p + \frac{1}{\rho}\nabla\cdot\boldsymbol{T}^{[\mathrm{s}]} + \frac{1}{\rho}\nabla\cdot\boldsymbol{T}^{[\mathrm{p}]}, \tag{2.1}$$

where $\boldsymbol{u}(\boldsymbol{x},t)$ is velocity, ρ is density, $p(\boldsymbol{x},t)$ is pressure, $\boldsymbol{T}^{[\mathrm{s}]}(\boldsymbol{x},t)=2\beta\mu\boldsymbol{S}$ is the Newtonian stress due to the solvent, μ and $\beta\mu$ are the mixture and solvent molecular viscosities, $\boldsymbol{S}$ is the rate-of-strain tensor, $\boldsymbol{T}^{[\mathrm{p}]}(\boldsymbol{x},t)$ is the polymer stress given by (Bird, Armstrong & Hassager 1987)

$$\boldsymbol{T}^{[\mathrm{p}]} = \tilde{n}(\boldsymbol{x},t)k_{\mathrm{B}}T(f(r)\boldsymbol{C}-\boldsymbol{I}), \tag{2.2}$$

$\tilde{n}(\boldsymbol{x},t)$ is the number density of polymer molecules, k_{B} is the Boltzmann constant, T is temperature, $\boldsymbol{C}$ is the conformation tensor, $\boldsymbol{I}$ is the identity tensor, $r\equiv\sqrt{\mathrm{Tr}\{\boldsymbol{C}\}}$ is the locally averaged end-to-end distance of the polymer chains, $f(r)=(L^2-3)/(L^2-r^2)$ is the nonlinear spring force and L^2 is the maximum extensibility parameter. $\boldsymbol{T}^{[\mathrm{p}]}$ can be written in terms of a polymer relaxation time, λ_{p} (Bird *et al.* 1987):

$$\boldsymbol{T}^{[\mathrm{p}]} = n(\boldsymbol{x},t)(1-\beta)\frac{\mu}{\lambda_{\mathrm{p}}}(f(r)\boldsymbol{C}-\boldsymbol{I}), \tag{2.3}$$

where $n(\boldsymbol{x},t)\equiv\tilde{n}(\boldsymbol{x},t)/n_0$ is a normalized concentration (i.e. a uniformly mixed polymer system corresponds to $n(\boldsymbol{x},t)=1$) and $(1-\beta)\mu/\lambda_{\mathrm{p}}=n_0k_{\mathrm{B}}T$ relates the polymer relaxation time to the bulk average polymer concentration, n_0. The conformation tensor and normalized concentration satisfy

$$\frac{\mathrm{D}\boldsymbol{C}}{\mathrm{D}t} = \boldsymbol{C}\cdot\nabla\boldsymbol{u} + \nabla\boldsymbol{u}^{\mathrm{T}}\cdot\boldsymbol{C} - \frac{[f(r)\boldsymbol{C}-\boldsymbol{I}]}{\lambda_{\mathrm{p}}}, \tag{2.4}$$

$$\frac{\mathrm{D}n}{\mathrm{D}t} = \mathscr{D}\nabla^2 n, \tag{2.5}$$

where $\mathscr{D}$ is the mass diffusivity of the polymer.

We consider turbulence in a Cartesian box of aspect ratio 2:1:1 in the x-, y- and z-directions (see figure 1*a*). We subject the turbulence to a mean velocity

Case	λ_p	$We_{\mathscr{S}}$	L^2	r_{cr}^2
A	0.050	1.41	10 000	28.6
B	0.075	2.12	10 000	46.7
C	0.100	2.83	10 000	66.4
C1	0.100	2.83	40 000	260.0
D	0.125	3.54	10 000	87.6

TABLE 1. Summary of the parameters used in the DNS. The initial turbulence parameters were: $q^2 \equiv \langle \boldsymbol{u}' \cdot \boldsymbol{u}' \rangle = 15.4$, $\epsilon = 106.9$ is the dissipation rate, $\ell = 0.116$ is the integral length scale, $\nu = 0.015$ is the kinematic viscosity and $\mathscr{S} = 28.3$ is the shear rate, where the numerical values are given in consistent arbitrary units. These quantities correspond to a Taylor-microscale Reynolds number $R_\lambda \equiv q^2/3\sqrt{15/\nu\epsilon} = 15.8$ and dimensionless shear parameter $S^* \equiv \mathscr{S} q^2/\epsilon = 4.1$. Note that $\beta = 0.95$ and $Sc \equiv \nu/\mathscr{D} = 0.7$ throughout. The concentration variable, n, was initially set to 9.85 within the polymer layer.

$\overline{\boldsymbol{u}} = (\overline{u}, \overline{v}, \overline{w}) = (\mathscr{S} y, 0, 0)$, where $\mathscr{S}$ is the constant mean shear rate. The boundary conditions are periodic in the x- and z-directions, and shear periodic in the y-direction (e.g. see Rogallo 1981). The initial velocity field is solenoidal Gaussian fluctuations with an energy spectrum that follows a k^2 power law at lower wavenumbers, a $k^{-5/3}$ power law at higher wavenumbers, with a peak at $k = 10$, chosen so that the longest integral length scale never exceeds 10 % of the box size during the analysed period of each simulation. We verify small-scale resolution by the requirement that $k_{max}\eta \geqslant 1.1$ (k_{max} is the highest resolved wavenumber in the simulation and $\eta = (\nu^3/\epsilon)^{1/4}$ is the Kolmogorov scale). In order to guarantee good resolution at both large and small scales, the initial Taylor Reynolds number was 16, growing to approximately 50 at $\mathscr{S} t = 10$, when the data were analysed.

The polymer concentration is initially set to $n = 9.85$ within a slab in the x–z plane at the centre of the box that is 13 grid spacings thick in the y-direction, and zero outside (see figure 1*a*). The polymer properties can be expressed in terms of four dimensionless parameters: the Weissenberg number $We_{\mathscr{S}} \equiv \mathscr{S}\lambda_p$; the dimensionless maximum extensibility parameter L^2; the concentration parameter β; and the Schmidt number $Sc \equiv \nu/\mathscr{D}$. Table 1 shows the values of the polymer parameters that were applied in this study. The choices of Weissenberg number and L^2 correspond to linear polyethyleneoxide at molecular weights of 2–4 million in an aqueous boundary layer with a free-stream velocity of order 10–20 m s^{-1} (e.g. a mid-size ship at top speed). Although polymers of this molecular weight have Schmidt numbers of order 10^6, scalars at such large Schmidt numbers cannot be resolved in a DNS (Yeung, Sykes & Vedula 2000). Instead we set $Sc = 0.7$ to ensure a well-resolved scalar field. Dimitropoulos *et al.* (2006) studied the effect of Schmidt number on polymer mixing in a boundary layer by comparing DNS with $Sc = 1$ to a large-eddy simulation (LES) with $Sc = 1000$. The data showed significant sensitivity of the mean polymer concentration to Sc in the viscous layer near the wall, but found relative insensitivity in the buffer region that more closely corresponds to our turbulent shear simulations. Comparisons between turbulent boundary layer experiments (Delo, Kelso & Smits 2004) using fluorescein dye in water ($Sc \sim 10^3$) and DNS (Yeung, Brasseur & Bell 1993) with a passive scalar ($Sc \sim 1$) show that the large-scale structure is nearly identical, with the effect of Sc only significant at the diffusion-dominated small scales. As discussed in Robert *et al.* (2007), we prestretch the polymer to allow its effect to be observed within the time window of the simulations. The initial conformation tensor was set to $\boldsymbol{C} = r_{cr}^2(1 + 0.2\gamma)\boldsymbol{I}$,

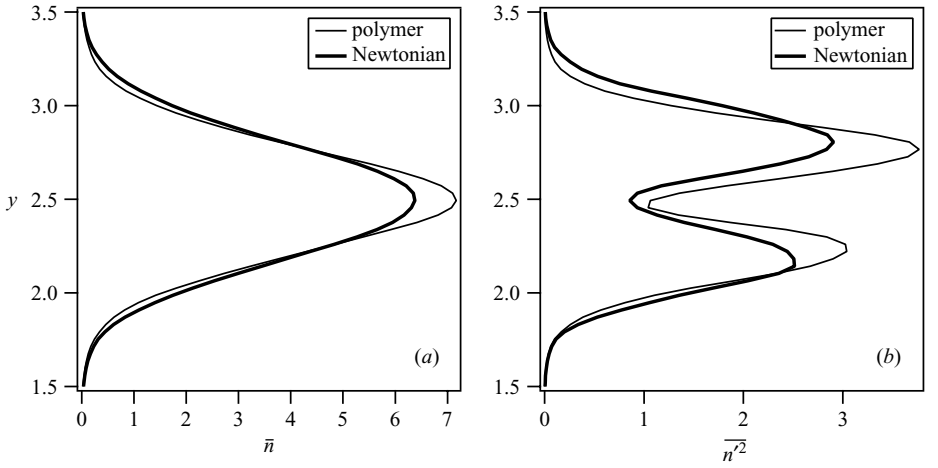

FIGURE 2. Mean (normalized) polymer concentration (a) and polymer concentration variance (b) across the mixing layer for Case A at dimensionless time $\mathscr{S}t = 10$. Thicker lines are the equivalent curves for a passive scalar in Newtonian turbulence.

γ is a uniform random variable over $[-1, 1]$ for each diagonal element of $\boldsymbol{C}$ and $r_{cr}^2 = [\frac{1}{2}\beta We_{\mathscr{S}} L^2]/[(1-\beta)L^2 + 3\beta We_{\mathscr{S}}]$. The values of r_{cr}^2 used are given in table 1.

Equation (2.4) is well known to be difficult to integrate numerically (Sureshkumar & Beris 1995; Vaithianathan & Collins 2003). The algorithm we use guarantees stability and accuracy. Further details can be found in Vaithianathan *et al.* (2006).

3. Results and discussion

Isocontours of the instantaneous polymer scalar field are shown in figure 1. At $\mathscr{S}t = 0$ (figure 1a), the polymer is concentrated in a thin band at the centre of the box. Turbulent mixing causes the band to thicken with time, while the maximum concentration decreases. Spatial averages in the mixing simulations were carried out on x–z planes, perpendicular to the mean velocity and scalar gradient directions. Some variability arises from the reduced sample compared with volume averages. Time averaging was precluded by non-stationarity. Calculations were carried out to $\mathscr{S}t = 12$, after which the integral length scale in the x-direction grew too large. All of the plots were calculated at $\mathscr{S}t = 10$.

Polymer mean concentration and concentration variance are shown in figure 2 (solid line) along with the equivalent quantity for an identically initiated passive scalar in Newtonian turbulence (thicker line). Spreading of the layer corresponds to a broadening of the mean scalar concentration $\bar{n}(y)$. Notice that the mean polymer concentration is more peaked and narrower than the corresponding passive scalar concentration, indicating that the polymer is diffusing more slowly than the passive scalar. Furthermore, the concentration variance for the passive scalar decays more rapidly than the polymer concentration variance.

The results shown in figure 2 suggest a reduction in the mixing rate of the polymer relative to the passive scalar. This is confirmed by figure 3, where the y-component of the turbulent polymer flux, $\overline{n'v'}$, is plotted as a function of y. The turbulent flux is a direct measure of the rate of spatial mixing of the polymer. In these plots, we explore the dependence of the scalar flux on the Weissenberg number (figure 3a) and polymer extensibility (figure 3b). In general, the effect of the polymer increases with both

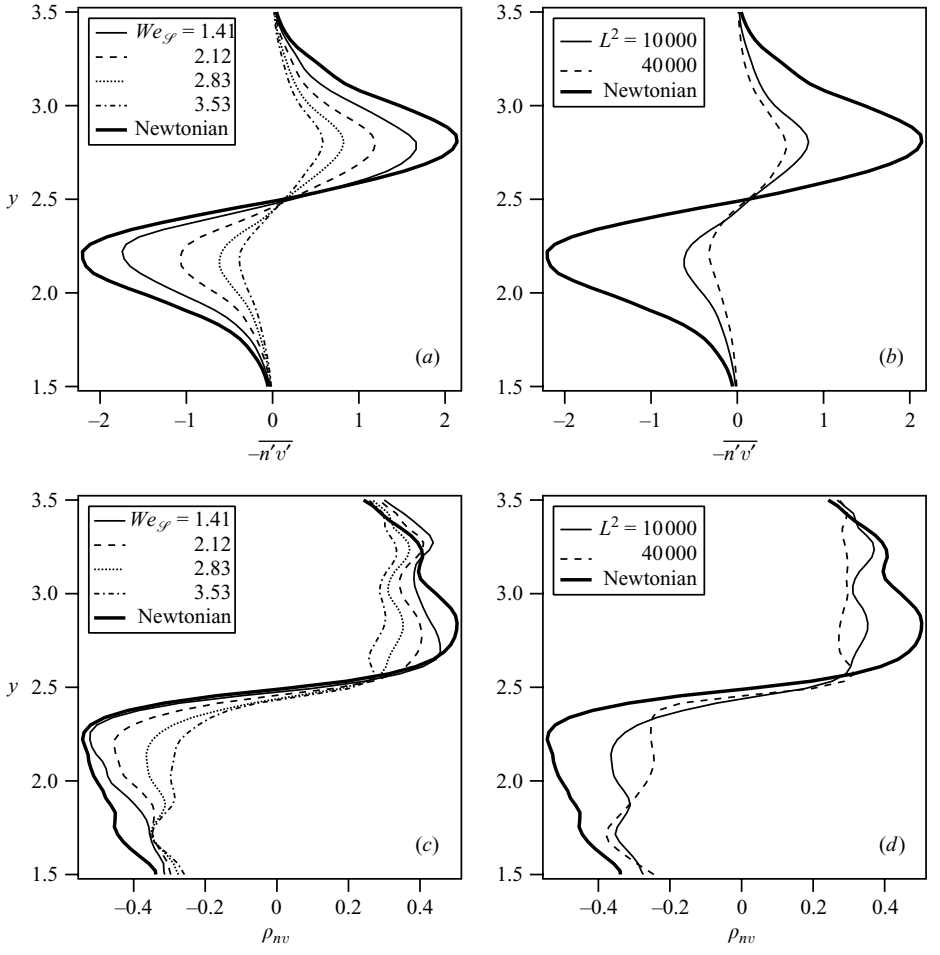

FIGURE 3. (*a*, *b*) Turbulent flux of polymer $-\overline{n'v'}$ across the mixing layer at $\mathscr{S}t = 10$. (*a*) Dependence on Weissenberg number (cases A, B, C and D in table 1); (*b*) dependence on L^2 (cases C and C1 in table 1). (*c*, *d*) Equivalent plots of the concentration–velocity correlation coefficient $\rho_{nv} \equiv -\overline{n'v'}/\sqrt{\overline{n'^2}\ \overline{v'^2}}$. Thicker lines are for a passive scalar in Newtonian turbulence.

parameters, causing a systematic decrease in the turbulent flux with increasing $We_{\mathscr{S}}$ and L^2. These results are in qualitative agreement with the observations of Gupta *et al.* (2005) for a passive tracer in drag-reduced turbulence, and recent experiments in a turbulent boundary layer with polymer injection (Somandepalli 2006).

Robert *et al.* (2007) found that the reduction in the Reynolds stress for uniform polymer concentration could be traced directly to the reduction in the vertical component of the velocity fluctuations, v'. We observe a similar reduction in v' near the centre of the polymer layer where the polymer concentration is high. The reduction in the turbulent flux of the polymer is expected to be strongly coupled to this reduction in v' (Gupta *et al.* 2005). Figures 3(*c*) and 3(*d*) show the correlation coefficient $\rho_{nv} \equiv -\overline{n'v'}/\sqrt{\overline{n'^2}\overline{v'^2}}$ for the two sets of parameters. Note the decrease in this coefficient near the centre of the box with increasing Weissenberg number and L^2, suggesting that the decrease in the scalar flux is due to more than just the suppression of v' that accompanies drag reduction.

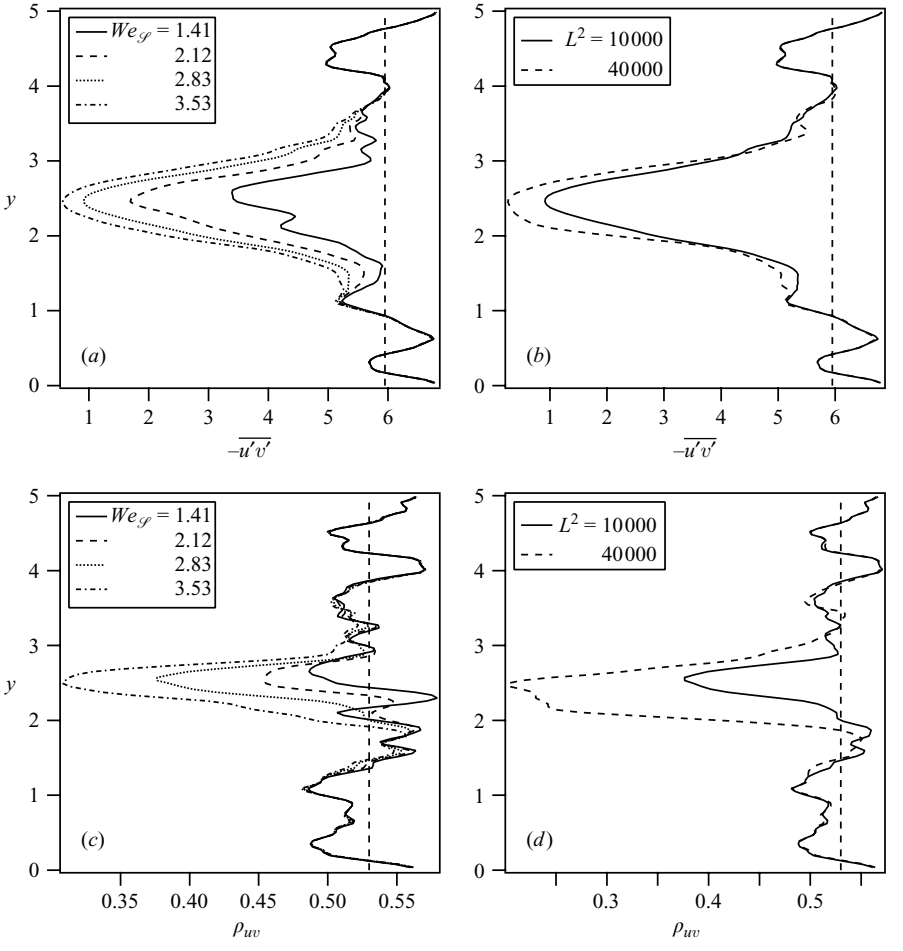

FIGURE 4. (*a*, *b*) Reynolds stress profiles at $\mathscr{S}t = 10$ for (*a*) cases A, B, C and D; (*b*) cases C and C1. (*c*, *d*) Equivalent plots of the correlation coefficient, $\rho_{uv} \equiv -\overline{u'v'}/\sqrt{\overline{u'^2}\overline{v'^2}}$. Vertical dashed lines are the volumetric average for the equivalent Newtonian shear flow.

Figure 4 shows the variation in the Reynolds stress profiles across the mixing layer at the indicated values of Weissenberg number (figure 4*a*) and L^2 (figure 4*b*). The Reynolds stress for the Newtonian flow is indicated by a vertical dashed line. The Reynolds stress near the centre of the polymer layer is strongly damped, while remaining Newtonian near the edges (to within the scatter). As the polymer spreads in the y-direction, so does Reynolds stress suppression. The damping near the centre is proportionately stronger due to the relatively high polymer concentration there. The u'–v' correlation coefficient (see figures 4*c* and 4*d*) is reduced in the polymer layer by an amount that depends strongly on the Weissenberg number and, to a lesser extent, on the extensibility parameter. This result is similar to those of Robert *et al.* (2007) who showed that the Reynolds stress, normalized by turbulent kinetic energy, is a decreasing function of Weissenberg number. The result is consistent with the turbulent scalar flux (figure 3) suggesting that, at higher $We_{\mathscr{S}}$, drag reduction involves both a reduction in the vertical velocity variance and a decorrelation of vertical velocity fluctuations from the other turbulence variables.

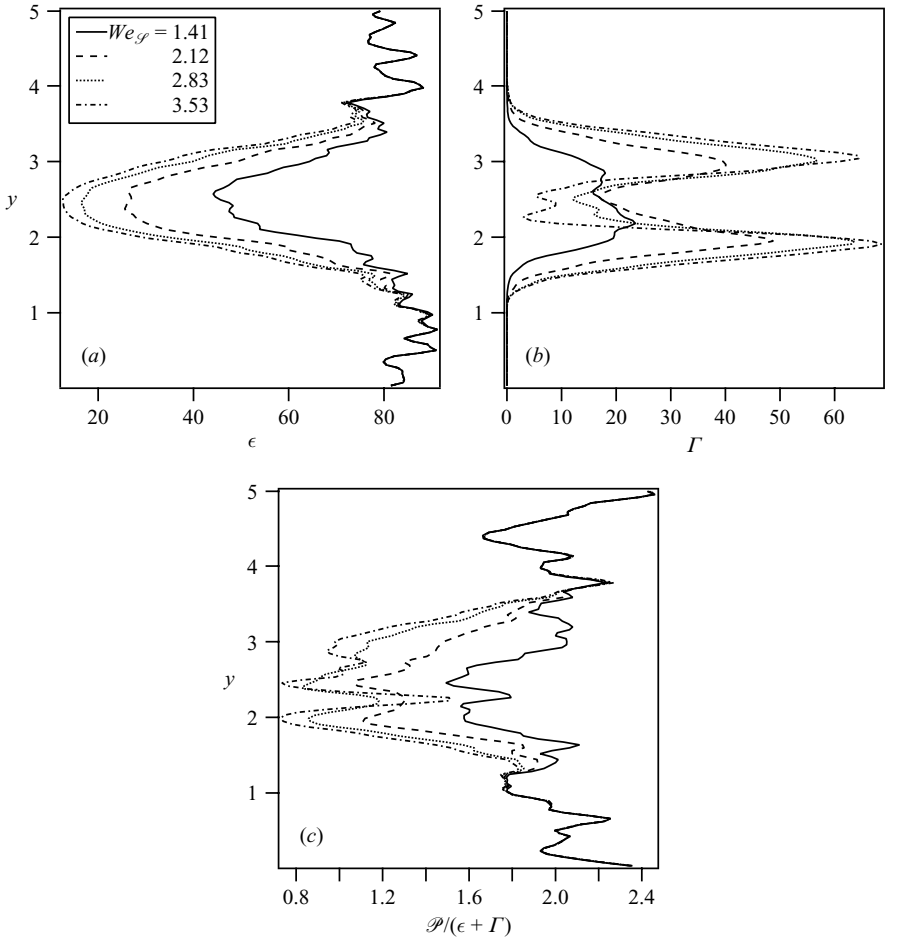

FIGURE 5. (*a*) Viscous dissipation; (*b*) polymer–turbulence energy exchange; and (*c*) ratio of production to the total energy drain at $\mathscr{S}t = 10$ for cases A, B, C and D.

The variation of viscous dissipation, $\epsilon \equiv 2\nu\overline{\boldsymbol{S} : \boldsymbol{S}}$, and polymer–turbulence energy exchange, $\Gamma \equiv \overline{\boldsymbol{T}^{[p]} : \boldsymbol{S}}/\rho$, are shown in figures 5(*a*) and 5(*b*) as a function of Weissenberg number. Viscous dissipation is increasingly suppressed in the polymer layer with increasing Weissenberg number. This is consistent with the uniform polymer results of Robert *et al.* (2007). However, the behaviour of the polymer–turbulence energy exchange, Γ, is more complex. At higher $We_{\mathscr{S}}$, turbulent kinetic energy (TKE) is transferred to polymer elastic energy principally at the edges of the mixing layer, where the turbulence is still relatively vigorous and capable of stretching the polymer in a region with significant polymer concentration. At the centre of the polymer layer, TKE is sufficiently damped to suppress polymer stretching, and therefore polymer–turbulence energy transfer. These results suggest the potential for the 'extinguishing' of polymer effects in local regions where TKE previously has been suppressed by the polymer. Figure 5(*c*) shows the ratio of the production of TKE, $\mathscr{P} \equiv -\overline{u'v'}\mathscr{S}$, to the total energy drain, $\epsilon + \Gamma$. Outside the polymer layer, where $\Gamma \ll \epsilon$, production over dissipation is very close to the Newtonian value of 2. However, in the polymer layer, there is a systematic decrease with increasing Weissenberg number. Moreover,

the value drops below unity for all but the lowest Weissenberg number, so that the TKE in the polymer layer would decay to zero in time without transport from the Newtonian regions outside the polymer layer.

Since the TKE in the polymer layer is growing (not shown), there must be a turbulent flux of energy from the outer edge to the centre to sustain the growth. A similar flux of stretched polymer is probably helping to sustain polymer stretch in the centre of the layer. We hypothesize that a similar mechanism may occur in wall-bounded polymer flows with injection. In that case, the relatively vigorous turbulence at the edge of the mixing layer would stretch the polymer chains that then are transported into the more concentrated polymer layer near the wall.

4. Conclusions

A numerical study of polymer mixing in drag-reduced turbulence was undertaken to better understand the interplay between turbulent energy changes due to polymers and mixing. Homogeneous turbulent shear flow was simulated with polymer confined initially to a thin slab in the centre of the computational domain. The calculations were terminated well before the polymer reached the edge of the computational domain and the periodic boundary conditions would have influenced the mixing.

We conclude that polymer–turbulence interactions suppress the rate of polymer mixing. In particular, the turbulent flux of polymer in the direction of the mean velocity gradient is increasingly reduced with increasing Weissenberg number and maximum extensibility parameter, L^2. This result is consistent with the observations of Gupta *et al.* (2005) that showed a reduction in the heat transfer in the wall-normal direction as a consequence of drag-reducing polymers. (They also found an augmentation in the turbulent flux in the streamwise direction, as did Dimitropoulos *et al.* (2006), that has no analogue in our simulations, since these are homogeneous in the streamwise and spanwise directions.)

We find that, at higher $We_{\mathscr{S}}$, the reduction in the turbulent scalar flux is due in part to the suppression of vertical velocity fluctuations, v', and in part due to a reduction in the correlation between vertical velocity fluctuations and polymer concentration fluctuations, suggesting an alteration in the turbulence structure that is more complex than simply the attenuation of $\overline{v'^2}$ by the action of the polymer. Our result is consistent with the recent experimental investigation of the scalar flux in turbulent boundary layers with polymer injection by Somandepalli (2006), that measured turbulent Schmidt numbers as large as 5. We also observe the potential for the quenching of polymer–turbulence interactions in regions where the TKE previously had been suppressed by the polymer.

The turbulence velocity statistics show a behaviour across the mixing layer that is similar to results found for uniform polymer concentrations (Robert *et al.* 2007). In the mixing layer, Reynolds stress is suppressed, as is viscous dissipation of TKE. The polymer–turbulence energy exchange, Γ, is zero in the Newtonian layer, peaks at the edge of the mixing layer, where there is a reasonably robust turbulence and a significant polymer concentration, and approaches a minimum in the centre of the mixing layer. This behaviour is qualitatively similar to the temporal dynamics of Γ in the uniform polymer case (Robert *et al.* 2007); Γ grows initially as the turbulence stretches the polymer, but eventually decays as the turbulence, weakened by polymer drag reduction, can no longer sustain the polymer stretch. An aspect of the present system that is not found in the homogeneous polymer case is the turbulent transport of TKE and stretched polymer from the edges of the mixing layer toward the centre.

This allows the TKE in the centre of the box to grow in time even though production divided by the energy drain, $\epsilon + \Gamma$, was suppressed below unity at higher Weissenberg numbers. This mechanism is probably present in wall-bounded flows with polymer injection, where polymer concentrations adjacent to the wall are sufficiently high to nearly completely damp the turbulence.

We acknowledge financial support from DARPA through the Friction Drag Reduction program, Contract No. NR0011-04-C-0010.

REFERENCES

Bewersdorff, H. W., Gry, A., Hoyer, K. & Tsinobėr, A. 1993 An investigation of possible mechanisms of heterogeneous drag reduction in pipe and channel flows. *Rheologica Acta* **32**, 140–149.

Bird, R. B., Armstrong, R. C. & Hassager, O. 1987 *Dynamics of Polymeric Liquids*, 2nd edn, Volume 2. Wiley.

Bonn, D., Amarouchene, Y., Wagner, C., Douady, S. & Cadot, O. 2005 Turbulent drag reduction by polymers. *J. Phys.: Condens. Matter* **17**, S1195–S1202.

Cadot, O., Bonn, D. & Douday, S. 1998 Turbulent drag reduction in a closed flow system: Boundary layer versus bulk effects. *Phys. Fluids* **10**, 426–436.

Cho, Y. I. & Hartnett, J. P. 1982 Heat transfer in flows with drag reduction. *Adv. Heat Transfer* **15**, 59–139.

De Angelis, E., Casciola, C. M., Benzi, R. & Piva, R. 2005 Homogeneous isotropic turbulence in dilute polymers. *J. Fluid Mech.* **531**, 1–10.

Delo, C. D., Kelso, R. M. & Smits, A. J. 2004 Three-dimensional structure of a low-Reynolds-number turbulent boundary layer. *J. Fluid Mech.* **512**, 47–83.

Dimitropoulos, C. D., Dubief, Y., Shaqfeh, E. S. G., Moin, P. & Lele, S. K. 2005 Direct numerical simulation of polymer-induced drag reduction in turbulent boundary layer flow. *Phys. Fluids* **17**, 011705.

Dimitropoulos, C. D., Dubief, Y., Shaqfeh, E. S. G., Moin, P. & Lele, S. K. 2006 Direct numerical simulation of polymer-induced drag reduction in turbulent boundary layer flow of inhomogeneous polymer solutions. *J. Fluid Mech.* **566**, 153–162.

Dubief, Y., White, C. M., Terrapon, V. E., Shaqfeh, E. S. G., Moin, P. & Lele, S. K. 2004 On the coherent drag-reducing and turbulence-enhancing behaviour of polymers in wall flows. *J. Fluid Mech.* **514**, 271–280.

Gupta, V. K., Sureshkumar, R. & Khomami, B. 2005 Passive scalar transport in polymer drag-reduced turbulent channel flow. *AIChE J.* **51**, 1938–1950.

Lee, M. J., Kim, J. & Moin, P. 1990 Structure of turbulence at high shear rate. *J. Fluid Mech.* **216**, 561–583.

L'vov, V. S., Pomyalov, A., Procaccia, I. & Tiberkevich, V. 2004 Drag reduction by polymers in wall bounded turbulence. *Phys. Rev. Lett.* **92**, 244503.

McComb, W. D. & Rabie, L. H. 1982 Local drag reduction due to injection of polymer solutions into turbulent flow in a pipe. *AIChE J.* **28**, 547–557.

Min, T., Yoo, J. Y., Choi, H. & Joseph, D. D. 2003 Drag reduction by polymer additives in a turbulent channel flow. *J. Fluid Mech.* **486**, 213–238.

Peterlin, A. 1961 Streaming birefringence of soft linear macromolecules with finite chain length. *Polymer* **2**, 257–264.

Petrie, H. L. & Fontaine, A. A. 1996 Comparison of turbulent boundary layer modification with slot-injected and homogeneous drag-reducing polymer solutions. In *ASME Fluid Engineering Division Summer Meeting*, FED 237, pp. 205–210.

Ptasinski, P. K., Boersma, B. J., Nieuwstadt, F. T. M., Hulsen, M. A., Van den Brule, B. H. A. A. & Hunt, J. C. R. 2003 Turbulent channel flow near maximum drag reduction: Simulations, experiments and mechanisms. *J. Fluid Mech.* **490**, 251–291.

Robert, A., Vaithianathan, T., Collins, L. R. & Brasseur, J. G. 2007 Fundamental physics underlying polymer drag reduction from DNS of homogeneous turbulence with the FENE-P model. *J. Fluid Mech.* (in review).

ROGALLO, R. S. 1981 Numerical experiments in homogeneous turbulence. *Technical Report* 81315. NASA.

SOMANDEPALLI, V. S. R. 2006 Combined PIV and PLIF measurements in a polymer drag reduced turbulent boundary layer. PhD thesis Stanford University.

SURESHKUMAR, R. & BERIS, A. N. 1995 Effect of artificial stress diffusivity on the stability of numerical calculations and the flow dynamics of time-dependent viscoelastic flows. *J. Non-Newtonian Fluid Mech.* **60**, 53–80.

SURESHKUMAR, R., BERIS, A. N. & HANDLER, R. A. 1997 Direct numerical simulation of turbulent channel flow of a polymer solution. *Phys. Fluids* **9**, 743–755.

VAITHIANATHAN, T. & COLLINS, L. R. 2003 Numerical approach to simulating turbulent flow of a viscoelastic polymer solution. *J. Comput. Phys.* **187**, 1–21.

VAITHIANATHAN, T., ROBERT, A., BRASSEUR, J. G. & COLLINS, L. R. 2006 An improved algorithm for simulating three-dimensional, viscoelastic turbulence. *J. Non-Newtonian Fluid Mech.* **140**, 3–22.

VIRK, P. S. 1975 Drag reduction fundamentals. *AIChE J.* **21**, 625–656.

YEUNG, P. K., BRASSEUR, J. G. & BELL, D. M. 1993 Evolution of passive scalar sources in a numerically simulated boundary layer. In *Near Wall Turbulent Flows* (ed. R. M. C. So, C. G. Speziale & B. E. Launder), pp. 307–316. Elsevier.

YEUNG, P. K., SYKES, M. C. & VEDULA, P. 2000 Direct numerical simulation of differential diffusion with Schmidt number up to 4.0. *Phys. Fluids* **12**, 1601–1604.

YOON, H. K. & GHAJAR, A. J. 1987 Heat eddy diffusivity for viscoelastic turbulent pipe flow. *Intl Commun. Heat Mass Transfer* **14**, 237–249.